Eur. Phys. J. C (2023) 83:171
https://doi.org/10.1140/epjc/s10052-023-11320-5

THE EUROPEAN PHYSICAL JOURNAL C

Regular Article - Theoretical Physics

Signatures of regular black holes from the quasar continuum spectrum

Indrani Banerjee[a]

Department of Physics and Astronomy, National Institute of Technology, Rourkela, Odisha 769008, India

Received: 5 November 2022 / Accepted: 12 February 2023

Abstract Regular black holes arising in Einstein gravity coupled to non-linear electrodynamics are worth studying as they can circumvent the $r = 0$ curvature singularity arising in general relativity. In this work we explore the signatures of regular black holes with a Minkowski core from the quasar continuum spectrum. We use thin-disk approximation to derive the theoretical luminosity from the accretion disk and compare it with the optical data of eighty Palomar Green quasars. Our analysis based on error estimators like the χ^2, the Nash–Sutcliffe efficiency, the index of agreement etc. reveal that optical observations of quasars favor black holes with a small non-linear electrodynamics charge parameter $k \simeq 0.15$ although the Kerr scenario is allowed within $2-\sigma$ interval. The implications are discussed.

1 Introduction

The success of general relativity (GR) in explaining observations at all length scales makes it the most widely accepted theory of gravity till date [1–3]. With two successive ground breaking discoveries, namely, the gravitational waves from merging compact binaries [4–8] and the image of black holes [9–15], the theory has received observational confirmation in the strong field regime as well. Despite its astounding success, the theory has certain shortcomings, e.g it cannot explain the flat rotation curves of galaxies and the accelerated expansion of the universe [16–20] and is marred with singularities [21] associated with the big bang and black holes. This has given birth to a large number of alternatives to GR, which involves modification in the gravity sector, addition of extra fields in the matter sector or both [22–36].

The celebrated theorems of Hawking and Penrose [21] state that spacetime singularities are inevitable in GR. It is believed that suitable quantum gravity models can evade the $r = 0$ curvature singularity present in general relativistic black holes. However, the quantum nature of gravity continues to be an ill-understood subject till date [37–45]. In the absence of a well accepted theory of quantum gravity, the black hole singularity issue can be addressed classically by invoking regular black holes [46–48]. One possible scenario where such black hole solutions arise comprise of Einstein gravity coupled to non-linear electrodynamics. Such black holes have a horizon surrounding $r = 0$ and the curvature invariants are finite at all points in spacetime [49–56]. The core at $r = 0$ often assumes a de Sitter character [57–59] which has been studied quite extensively. It is believed that such a black hole may be formed when unlimited increase of spacetime curvature during a stellar collapse gets halted due to quantum fluctuations.

Apart from a de Sitter nature, the core at $r = 0$ may also be of Minkowski type which arises as solution of Einstein's equations with an anisotropic fluid as the source. Such a fluid obeys the weak energy condition and resembles the Maxwell's stress tensor far from the black hole [60]. The electric field therefore resembles the Coulomb field and the static, spherically symmetric metric assumes the form of the Reissner Nordström spacetime at large distances from the source. Investigating the observational characteristics of such a spacetime is important as the mass of the black hole has an exponential convergence factor which makes the quantum gravity model associated with the classical theory finite to all orders [61]. Studying a finite quantum gravity theory is important as it can not only address the singularity issues in GR, but can also resolve the cosmological constant problem [62] and eradicate the divergences arising in flat space quantum field theories.

Since we are interested in exploring the observational properties of the regular black hole with a Minkowski core, we consider the stationary, axisymmetric counterpart of the aforesaid spacetime. The rotating solution is obtained by

[a] e-mail: banerjeein@nitrkl.ac.in (corresponding author)

Published online: 22 February 2023

applying the Newman–Janis algorithm [63] or other mathematical techniques [64–66] to the static, spherically symmetric seed metric. This has been worked out by Ghosh [67] which we use in this work. Needless to say, such a spacetime has a horizon covering the $r = 0$ Minkowski core and resembles the Kerr–Newman metric at large distances from the source [67]. The observational signatures of regular black holes have been studied extensively [68–78].

The goal of the present work is to decipher the imprints of the aforesaid spacetime from the continuum spectrum of a sample of eighty Palomar Green quasars [79]. We assume that these quasars are regular black holes with a Minkowski core arising in Einstein gravity coupled to non-linear electrodynamics. Considering the rotating solution [67] we derive the luminosity from the accretion disk of these quasars in the thin-disk approximation [80,81] and compare it with their observed optical luminosities. This in turn enables us to establish constrains on the non-linear electrodynamics charge parameter supposed to be associated with the quasars. Our analysis is based on error estimators like the chi-square, the Nash–Sutcliffe efficiency, the index of agreement and their modified forms. We also provide independent estimates of spin for some of the quasars.

We organise the paper in the following way: Sect. 2 is dedicated in describing the regular black holes with a Minkowski core. In Sect. 3 we derive the theoretical luminosity from the accretion disk in the aforesaid background using thin-disk approximation. The theoretical optical luminosity is then compared with the observed ones using the error estimators in Sect. 4. We conclude with a summary of our results with some scope for future work in Sect. 5. Here we assume (−,+,+,+) as metric convention and work with geometrized units which considers G=c=1.

2 Regular black holes with a Minkowski core

In this section we describe regular black holes with an asymptotically Minkowski core which arise in Einstein gravity coupled to non-linear electrodynamics [48,68,82–85]. The action associated with non-linear electrodynamics coupled to Einstein gravity is given by [48,68,82–85],

$$S = \int d^4x\sqrt{-g}\left(\frac{R}{16\pi} - \frac{L(F)}{4\pi}\right) \tag{1}$$

where R refers to the Ricci scalar, $L(F)$ the non-linear electrodynamics Lagrangian density with $F = F^{ab}F_{ab}/4$ the Faraday invariant, $F_{ab} = \partial_a A_b - \partial_b A_a$ the electromagnetic field strength tensor and A_i the gauge field. In this work the Lagrangian density associated with non-linear electrodynamics is given by [68],

$$L(F) = Fe^{-\alpha(2g^2F)^{1/4}} \tag{2}$$

where $\alpha = g/(2\mathcal{M})$ with g the magnetic charge and $\mathcal{M}$ the mass of the black hole.

In this case, Einstein's equations is sourced by an anisotropic fluid whose energy-momentum tensor assume the form:

$$\begin{aligned} T_0^0 &= -\rho(r) = \frac{-\mathcal{M}k}{4\pi r^4}e^{-k/r}; \\ T_1^1 &= -\rho(r) = \frac{-\mathcal{M}k}{4\pi r^4}e^{-k/r}; \\ T_2^2 &= T_3^3 = \frac{\mathcal{M}k}{4\pi r^4}\left(1 - \frac{k}{2r}\right)e^{-k/r} \end{aligned} \tag{3}$$

with $k = g^2/(2r_g^2)$ where $r_g = G\mathcal{M}/c^2$ is the gravitational radius. It is interesting to note that the energy momentum tensor in (3) is consistent with the weak energy condition and resembles the Maxwell stress tensor far from the source [86].

With the source being given by Eq. (3) the static, spherically symmetric and asymptotically flat, black hole solution of Einstein's equations assume the form,

$$\begin{aligned} ds^2 = &-(1 - \frac{2\mathcal{M}}{r}e^{-k/r})dt^2 + \frac{dr^2}{1 - \frac{2\mathcal{M}}{r}e^{-k/r}} \\ &+ r^2d\theta^2 + r^2sin^2\theta d\phi^2 \end{aligned} \tag{4}$$

Since we are interested in studying astrophysics of these black holes, we need to consider the rotating counterpart of Eq. (4). This is obtained by applying the Newman–Janis algorithm [63–66] to the above static, spherically symmetric seed metric [67,68]. This gives rise to the stationary, axisymmetric counterpart of Eq. (4) which in Boyer–Lindquist coordinates is given by,

$$\begin{aligned} ds^2 = &-\left(1 - \frac{2M(r)r}{\Sigma}\right)dt^2 - \frac{4aM(r)r}{\Sigma}\sin^2\theta dtd\phi \\ &+ \frac{\Sigma}{\Delta}dr^2 + \Sigma d\theta^2 + \left(r^2 + a^2 + \frac{2M(r)ra^2}{\Sigma}\sin^2\theta\right) \\ &\times \sin^2\theta d\phi^2 \end{aligned} \tag{5}$$

where,

$$\Sigma = r^2 + a^2\cos^2\theta\ ,\ \Delta = r^2 + a^2 - 2M(r)r \tag{6}$$

and a is the angular momentum of the black hole. In Eq. (5), $M(r)$ is the mass function given by,

$$M(r) = \mathcal{M}e^{-k/r} \tag{7}$$

which becomes $\mathcal{M}$ as $r \to \infty$. $M(r)$ can be thought of as mass inside the sphere of radius r. In this context it may be worth mentioning that in [87] the authors studied the Penrose process in black holes arising in Einstein–Maxwell dilaton axion gravity. There the axion field was responsible for endowing angular momentum to the black hole. Gravity coupled to non-linear electrodynamics along with axion and dilaton have been studied in the context of Born–Infeld gravity [88] although the black hole solution in such a theory has not been obtained. In the present work the Lagrangian density does not contain couplings of axion or dilaton field. Here the gauge field A_μ renders rotation to the black hole. It would be interesting to explore the implications of dilaton-axion coupled Einstein gravity in non-linear electrodynamics on black hole solutions. Once the black hole solution is obtained one can study the associated observational signatures and thermodynamics. This however is outside the scope of the present discussion and we leave it for future work.

It is important to note that the metrics in eqs. (4) and (5) are regular at all points in the spacetime. At $r = 0$, the energy density vanishes unlike black holes with a de Sitter core where the energy density becomes constant at $r = 0$. Moreover, the metric in Eq. (4) or Eq. (5) reduces to the Minkowski background at $r = 0$. When $k = 0$, the metric in eq. (4) resembles the Schwarzschild spacetime while the metric in (5) reduces to the Kerr spacetime. For a non-zero k with large r, in the limit $r \gg k$, $M(r) = \mathcal{M} - \frac{Q^2}{2r}$ and the metric in Eq. (5) assumes the form of the Kerr–Newman spacetime. Studying the regular solution in Eq. (4) or Eq. (5) is worthwhile as the curvature invariants become immensely simpler than black hole spacetimes with a regular de Sitter core, e.g. Bardeen metric, and bears several physically interesting features defined by the Lambert W function [86,89–95].

The event horizon of the spacetime given by Eq. (5) has a spherical topology and is obtained by solving for r in the equation,

$$g^{rr} = \Delta = r^2 + a^2 - 2r\mathcal{M}e^{-k/r} = 0 \tag{8}$$

The existence of an event horizon requires one to solve for real, positive values of r in Eq. (8). The requirement of an event horizon or a black hole solution imposes restrictions on the values of k and a, [96] such that $0 \lesssim k \lesssim 0.7$ and for every k, the spin a lies in a certain range. In the present work we shall constrain both k and a from the quasar continuum spectrum.

3 Continuum spectrum from the accretion disk in a stationary, axisymmetric spacetime

The continuum spectrum emitted by the accretion disk surrounding a black hole is sensitive to the background spacetime and the properties of the accretion flow. Therefore it serves as an important astrophysical tool to decipher the nature of the background metric. Consider the stationary, axisymmetric spacetime which is asymptotically flat and has reflection symmetry,

$$ds^2 = g_{tt}dt^2 + 2g_{t\phi}dtd\phi + g_{\phi\phi}d\phi^2 + g_{rr}dr^2 + g_{\theta\theta}d\theta^2 \,, \tag{9}$$

For such a spacetime the metric components are independent of t and ϕ, such that we have two conserved quantities, namely specific energy $\mathcal{E}$ and specific angular momentum $\mathcal{L}$ which for timelike particles are respectively given by,

$$\mathcal{E} = \frac{-g_{tt} - \Omega g_{t\phi}}{\sqrt{-g_{tt} - 2\Omega g_{t\phi} - \Omega^2 g_{\phi\phi}}} \tag{10}$$

$$\mathcal{L} = \frac{\Omega g_{\phi\phi} + g_{t\phi}}{\sqrt{-g_{tt} - 2\Omega g_{t\phi} - \Omega^2 g_{\phi\phi}}} \tag{11}$$

where, Ω is the angular velocity of massive test particles,

$$\Omega = \frac{d\phi}{dt} = \frac{-g_{t\phi,r} \pm \sqrt{(-g_{t\phi,r})^2 - (g_{\phi\phi,r})(g_{tt,r})}}{g_{\phi\phi,r}} \tag{12}$$

It is important to note that we consider motion along the equatorial plane such that $\mathcal{E}$ and $\mathcal{L}$ are functions of r and the conserved quantities are independent of $g_{\theta\theta}$.

In this section we shall derive the continuum spectrum from the accretion disk surrounding a rotating black hole with line element given by Eq. (9). While deriving the spectrum we shall consider the thin-disk approximation [80,81] where the accretion flow is confined along the equatorial plane ($\theta = \pi/2$). As matter inspirals and falls into the central black hole the azimuthal velocity v_ϕ far exceeds the radial velocity v_r and the vertical velocity v_z such that $v_\phi \gg v_r \gg v_z$. Because of this condition, the system does not harbor outflows and motion is roughly along circular geodesics. The presence of viscosity in the system endows minimal radial velocity to the accreting fluid, such that the matter slowly inspirals and falls into the black hole. Due to circular geodesic motion along the equatorial plane the disk height $h(r) \ll r$ where r is the radial distance from the central black hole. The energy-momentum tensor of the accreting fluid assumes the form,

$$\mathcal{T}^\mu_\nu = \rho(1 + \Pi)u^\mu u_\nu + s^\mu_\nu + u^\mu v_\nu + v^\mu u_\nu \tag{13}$$

where ρ is the proper density and u_ν the four velocity of the accreting fluid. In Eq. (13) Π represents the specific internal energy of the accreting fluid such $\rho\Pi u^\mu u_\nu$ is the dissipation term. The thin-disk approximation implies that $\Pi \ll 1$ which in turn ascertains that the rest energy of the accreting fluid far supercedes the dissipation effects. As a consequence, special relativistic effects due to local thermodynamic, hydrody-

namic and radiative properties of the flow can be neglected and no heat is retained with the flow. However, the general relativistic effects due to the black hole continues to play a conspicuous role. $s^{\mu\nu}$ is associated with the the stress-tensor while v^{μ} represents the energy flux relative to the local inertial frame. Note that $s^{\mu\nu}$ and v^{μ} are orthogonal to the 4-velocity, i.e., $s_{\mu\nu}u^{\mu} = 0 = v_{\mu}u^{\mu}$. The photons generated due to viscous dissipation interacts very efficiently with the accreting fluid before leaving the system as v^z. Thus, every annulus of the disk emits a black body radiation such that the continuum spectrum from the accretion disk in the thin-disk approximation represents a multi-color black body spectrum.

We now aim to calculate the flux and subsequently the luminosity from the accretion disk in the thin-disk approximation. We shall assume that accretion takes place at a steady rate $\dot{M}$ which is very small compared to the mass of the black hole such that the process of accretion does not change the black hole mass over the timescales of interest. The metric therefore continues to remain stationary and axisymmetric and is given by Eq. (5). The equation governing conservation of mass is given by,

$$\dot{M} = -2\pi\sqrt{-\gamma}u^{r}\Sigma \tag{14}$$

where u_r is the radial velocity, $\Sigma = \int \rho dz$ is the average surface density of the accreting fluid and γ is the determinant of the two dimensional metric associated with the equatorial plane such that $\gamma = -g_{rr}(g_{t\phi}^2 - g_{tt}g_{\phi\phi})$. The accretion flow also conserves angular momentum and energy. These are best described by defining a current J_i^{ν} where $i \equiv t, \phi$ corresponding to energy and angular momentum respectively. The conservation of energy thus assumes the form

$$\nabla_{\nu}J_t^{\nu} = \nabla_{\nu}\left\{T_{\mu}^{\nu}\left(\frac{\partial}{\partial t}\right)^{\mu}\right\} = \partial_r(\dot{M}\mathcal{E} - 2\pi\sqrt{-\gamma}\Omega w_{\phi}^{r}) - 4\pi\sqrt{-\gamma}\mathcal{F}\mathcal{E} = 0 \tag{15}$$

while the conservation of angular momentum is governed by,

$$\nabla_{\nu}J_{\phi}^{\nu} = \nabla_{\nu}\left\{T_{\mu}^{\nu}\left(\frac{\partial}{\partial \phi}\right)^{\mu}\right\} = \partial_r(\dot{M}\mathcal{L} - 2\pi\sqrt{-\gamma}w_{\phi}^{r}) - 4\pi\sqrt{-\gamma}\mathcal{F}\mathcal{L} = 0 \tag{16}$$

In Eq. (15) and Eq. (16) w_{ϕ}^{r} refers to the height and time averaged stress tensor in the local rest frame of the accreting fluid,

$$w_{\beta}^{\alpha} = \int_{-h}^{h} dz\langle s_{\beta}^{\alpha}\rangle \tag{17}$$

while $\mathcal{F}$ represents the flux radiated from the accretion disk,

$$\mathcal{F} \equiv \langle v^z(r,h)\rangle = \langle -v^z(r,-h)\rangle \tag{18}$$

For a detailed derivation of the conservation laws one is referred to [80,81]. From the conservation laws one can derive an analytic expression for the flux [81] which assumes the form,

$$\mathcal{F} = \frac{\dot{M}}{4\pi\sqrt{-\gamma}}f \quad \text{where} \tag{19}$$

$$f = -\frac{\Omega_{,r}}{(\mathcal{E}-\Omega\mathcal{L})^2}\left[\mathcal{E}\mathcal{L} - \mathcal{E}_{ms}\mathcal{L}_{ms} - 2\int_{r_{ms}}^{r}\mathcal{L}\mathcal{E}_{,r'}dr'\right] \tag{20}$$

In Eq. (20), $\mathcal{E}_{ms}$ and $\mathcal{L}_{ms}$ correspond to the specific energy and specific angular momentum at the marginally stable circular orbit r_{ms}. It is important to note that while deriving $\mathcal{F}$ we assume that the viscous stress w_{ϕ}^{r} vanishes at r_{ms} such that the azimuthal velocity drops to zero and the accreting matter plunges into the black hole with pure radial velocity. In order to obtain the radius of the marginally stable circular orbit we need to understand the nature of the effective potential for motion of massive test particles. Such a potential is obtained from the equation $p^{\mu}p_{\mu} = -m^2$ and is given by,

$$V_{eff}(r) = \frac{\mathcal{E}^2 g_{\phi\phi} + 2\mathcal{E}\mathcal{L}g_{t\phi} + \mathcal{L}^2 g_{tt}}{g_{t\phi}^2 - g_{tt}g_{\phi\phi}} - 1 \tag{21}$$

Such a potential has an inflection point and the radius of the marginally stable circular orbit is obtained by solving for $V_{eff} = V'_{eff} = V''_{eff} = 0$ where prime denotes derivative with respect to r. The photons emitted in the disk due to viscous dissipation undergo repeated collisions with the accreting matter before leaving the system. Consequently each annulus of the disk emits a black body spectrum, such that the thin accretion disk is 'geometrically thin but optically thick'. The total emission from the disk is an envelope of the individual black body spectrum and is known as the multi-color black body spectrum. The temperature profile at any given radius therefore satisfies the Stefan-Boltzmann's law, $T(r) = \{F(r)/\sigma\}^{1/4}$ where σ is the Stefan-Boltzmann constant, and $F(r) = \mathcal{F}(r)c^6/G^2\mathcal{M}^2$. Therefore at every radius the disk emits a Planck spectrum, such that the luminosity from the disk at an observed frequency ν is given by,

$$L_{\nu} = 8\pi^2 r_g^2 \cos i \int_{r_{ms}}^{r_{out}} \sqrt{g_{rr}}B_{\nu}(T(r))r\, dr \tag{22}$$

While evaluating L_{ν} we make our radial coordinate dimensionless such that $r \equiv r/r_g$ where r_g is the gravitational radius given by $r_g = GM/c^2$. In Eq. (22) i is the inclination angle while the Plank spectrum is given by,

$$B_{\nu}(T(r)) = \frac{2h\nu^3}{c^2\left[exp(\frac{h\nu}{z_g kT(r)}) - 1\right]} \tag{23}$$

In Eq. (23),the gravitational redshift factor z_g associated with the outgoing photons is given by,

$$z_{\rm g} = E\frac{\sqrt{-g_{tt} - 2\Omega g_{t\phi} - \Omega^2 g_{\phi\phi}}}{E - \Omega L} \tag{24}$$

which takes into account the change in frequency suffered by the photon while travelling from the emitting medium to the observer [97]. In Eq. (24), E and L correspond to the specific energy and specific angular momentum of the outgoing photon.

One may note from Eq. (22) that L_ν is sensitive to the mass of the black hole, the accretion rate, the inclination angle and the metric components which are given by Eq. (5).

In Fig. 1 we plot the dependence of the luminosity from the accretion disk on frequency and the metric parameters k and a. We consider two sets of black holes masses, e.g. $\mathcal{M} = 10^7 M_\odot$ and $\mathcal{M} = 10^9 M_\odot$. For both the masses the accretion rate is taken to be $1 M_\odot$ year^{-1} while the inclination angle is assumed to be $i = \cos^{-1} 0.8$. We note from the figure that for any given mass the effect of the metric becomes conspicuous in the high frequency regime (spectra becomes distinguishable). This is because the high frequency part of the spectrum is emitted by the hot inner disk where the effect of the background metric is generally expected to be predominant. We further note from Fig. 1 that the accretion disk surrounding a lower mass black hole emits higher frequencies. This is because the temperature of the disk scales as $T(r) \propto \mathcal{M}^{-1/4}$. Therefore, a lower mass black hole has a hotter accretion disk and hence emits higher frequencies. In Fig. 1 the spectra denoted by black, blue and red lines correspond to $k = 0$, $k = 0.3$ and $k = 0.5$. In each case k and a are chosen in such a way that the event horizon remains real and positive [96]. The prograde spins are denoted by dashed lines, the retrograde spins are denoted by dotted lines while the non-rotating black holes are denoted by solid lines. It is important to note that for a given k the accretion disks of prograde black holes are much more luminous compared to non-spinning or retrograde black holes. This is because the inner edge of the disk (r_{isco}) from where the emission is maximum extends much closer (farther) to the black hole in case they are prograde (retrograde).

4 Contact with observations

In this section we compute the optical luminosity at 4861Å of a sample of eighty Palomar Green quasars studied in Davis and Laor [79] using the thin disk approximation. In order to compute the theoretical optical luminosity we need to provide information regarding the mass, inclination angle and the accretion rate Eq.(22). The masses of these quasars have been determined by reverberation mapping [98–101] and are reported in Davis and Laor [79]. For some quasars masses based on $M - \sigma$ method are also mentioned [79]. Here we shall consider masses determined by the method of reverberation mapping. Using the observed spectra in the optical [102], UV [103], far-UV [104], and soft X-ray [105] domain the bolometric luminosity of these quasars are estimated [79]. Supermassive black holes are multi-component systems comprising of the disk, the corona, the jet and the dusty torus [106]. The accretion disk of these systems generally emit in the optical/UV part of the spectrum. Since emission from the UV regime has maximum contribution to the error in the bolometric luminosity we shall consider the observed optical luminosity reported in Davis and Laor [79] for comparison with our theoretical estimates.

Apart from mass, information about the accretion rate and the inclination angle are required to obtain the theoretical optical luminosity. The accretion rates of these quasars are reported in [79]. In order to determine the accretion rate several theoretical models have been considered [79]. The base model turns out to be the so called TLUSTY model which uses stellar-atmosphere-like assumptions of the disk structure with spin $a = 0.9$. However, they also provide the degree of variation of the accretion rate if other disk models or black hole spins are used. For example, TLUSTY model with spin $a = 0$ results in 40% increment of the accretion rate for higher mass quasars and 10% increase in the accretion rate for low mass quasars compared to the base model. When black body model with $a = 0.9$ is used the accretion rates turn out to be lower by $10\% - 20\%$ for all quasars. Similarly when black body model with $a = 0$ is used the accretion rate of low mass quasars decrease by 20% while that of high mass quasars get enhanced by 40% compared to the base model. Therefore irrespective of the choice of model or black hole spin we vary the accretion rate between 80% to 140% of the value reported in [79] for all the PG quasars.

The quasar sample considered here are nearly face-on systems and therefore the inclination angle i is varied between $\cos i \in (0.5, 1)$ [79,107,108]. This is consistent with the estimates of [109] which reports the inclination angle for some quasars in the sample we are studying.

Having discussed the inputs we use for the calculation of theoretical optical luminosity (i.e., mass, accretion rate and inclination angle), we now describe the procedure we adopt to constrain the non-linear electrodynamics charge parameter k:

- We consider the eighty quasars to be regular black holes with a Minkowski core. Therefore these objects should possess an event horizon. This is ensured by solving for $\Delta = 0$ in Eq. (6). This gives us a theoretical restriction on the values of k and a such that $0 \lesssim k \lesssim 0.7$ and for every k, a lies in a certain range.

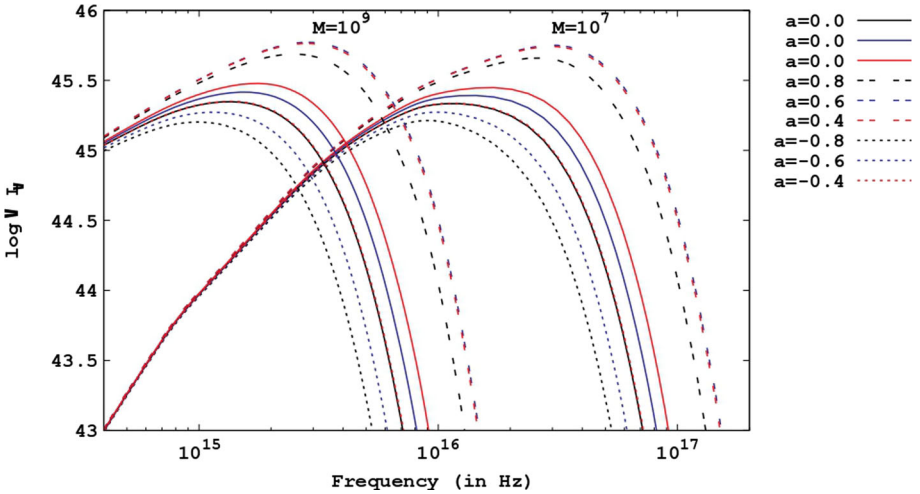

Fig. 1 The figure above depicts the variation of the theoretical luminosity from the accretion disk with frequency considering two sets of black hole masses, namely, $M = 10^9 M_\odot$ and $M = 10^7 M_\odot$. The inclination angle is taken to be $i = cos^{-1}0.8$ while the accretion rate assumed is $1 M_\odot$ year^{-1}. The black, blue and red lines correspond to $k = 0$, $k = 0.3$ and $k = 0.5$, where k is the non-linear electrodynamics charge parameter. Keeping k fixed, non-rotating black holes are represented by solid lines, while dashed and dotted lines correspond to prograde and retrograde black holes

- First of all, we choose a value of k between $0 \lesssim k \lesssim 0.7$. For the chosen k, the allowed range of a gets fixed.
- Next, we choose a quasar from the sample whose mass based on reverberation mapping is reported in [79].
- Keeping k and a fixed we now fix an inclination angle between $0.5 \lesssim \cos i \lesssim 1$.
- Keeping k, a and $cosi$ fixed we vary the accretion rate between $0.8\dot{M}$ to $1.4\dot{M}$, where $\dot{M}$ is the accretion rate obtained from the base model and reported in [79].
- For the chosen quasar and the given k we compute the theoretical luminosity at 4861Å for every combination of a, $\dot{M}$ and $\cos i$. The values of a, $\dot{M}$ and $\cos i$ which minimizes the error between the theoretical and the observed optical luminosities are noted and are referred to as a_{min}, $\dot{M}_{min}$ and $\cos i_{min}$ for the chosen quasar.
- We repeat steps 3–6 for all the quasars and estimate the errors as discussed in the next section.
- We then repeat steps 2–7 for all the values of k in the physically allowed range.

We next consider several error estimators to arrive at the most favorable magnitude of k derived from the optical observation of quasars.

4.1 Error estimators

- **Chi-square χ^2** : The χ^2 of a distribution is given by,

$$\chi^2(k) = \sum_{j=1}^{80} \frac{\left\{O_j - T_j\left(k, \{a_{min,j}, \cos i_{min,j}, \dot{M}_{min,j}\}\right)\right\}^2}{\sigma_j^2}. \tag{25}$$

where $\{O_j\}$ denotes the observed dataset and $T_j\left(k, \{a_{min,j}, \cos i_{min,j}, \dot{M}_{min,j}\}\right)$ represents the theoretical optical luminosity of the j^{th} quasar corresponding to a_{min}, $\cos i_{min}$ and $\dot{M}_{min}$ for a given k. The errors associated with the observed luminosity are denoted by σ_j. It is important to note that the errors corresponding to the observed optical luminosities of quasars are not given, therefore we use the errors associated with the bolometric luminosities [79] as the maximum possible error in the optical luminosity. From Eq. (25) it is easy to see that the value of k minimizing the χ^2 corresponds to the observationally favored magnitude of the non-linear electrodynamics charge parameter. The corresponding value of χ^2 is denoted by χ^2_{min}. Further, it is important to note that we do not minimize the χ^2 with respect to k, a, $\dot{M}$ and $cosi$ at the same time. This is because our primary goal is to determine the observationally favored value of the charge parameter k from the quasar optical data. Thus, although χ^2 depends on four parameters, the number of 'interesting parameters' is one (k) and there are three 'uninteresting parameters' (a, $\dot{M}$ and $cosi$) [110]. When we have only one 'interesting parameter' the 68%, 90% and 99% confidence intervals are determined by $\Delta\chi^2 = 1, 2.71, 6.63$ from χ^2_{min}. From eq. (22) we note that the theoretical luminosity depends both on the inner and the outer disk radius. The inner disk radius corresponds to r_{ms} (which depends on k and a) in the thin-disk approximation, whereas the outer disk radius is taken to be $r_{out} = 500 r_g$ and $r_{out} = 1000 r_g$. The luminosity from the accretion disk is much more sensitive to the inner radius (when the metric is asymptotically flat) and there-

fore calculating the errors by varying r_{out} is done just for completeness. The variation of χ^2 with k is shown in Fig. 2. From the figure it is clear that χ^2 minimizes for a small but non-trivial value of k ($k \simeq 0.15$) irrespective of the choice of r_{out}. This indicates that quasar optical data favors black holes in non-linear electrodynamics with a small magnetic monopole charge, compared to the Kerr scenario in GR. The 1-σ, 2-σ and 3-σ contours are denoted by black, blue and magenta lines. From Fig. 2 we note that when the 1-σ interval is considered the magnetic monopole charge parameter lies in the range $0.1 \lesssim k \lesssim 0.25$ for $r_{out} = 500r_g$ and in the range $0.05 \lesssim k \lesssim 0.32$ for $r_{out} = 1000r_g$. The Kerr scenario is however included within the 3-σ interval for $r_{out} = 500r_g$, while extending r_{out} to $1000r_g$ includes the Kerr scenario within 2-σ interval. It is important to note that for both choices of r_{out} large values of k are disfavored as they lie outside the 3-σ interval. We now consider a few more error estimators to validate our results based on χ^2 analysis.

- **Nash–Sutcliffe Efficiency:** The Nash–Sutcliffe Efficiency E [111–113] is given by the ratio of the squared difference between the observed and the theoretical luminosity to the squared difference between the observed and average luminosity subtracted from unity. The mathematical expression corresponding to the Nash–Sutcliffe Efficiency E is given by,

$$E(k) = 1 - \frac{\sum_j \left\{O_j - T_j\left(k, \{a_{min,j}, \cos i_{min,j}, \dot{M}_{min,j}\}\right)\right\}^2}{\sum_j \left\{O_j - O_{\rm av}\right\}^2} \tag{26}$$

Here, $O_{\rm av}$ denotes the average value of the observed optical luminosities of the PG quasars. While computing the differences in Eq. (26) we take logarithm of the observed, theoretical and average luminosity. From Eq. (26) it is easy to note that E can range from $-\infty$ to 1. A negative E implies that the mean of the observed data predicts the observation better than the theoretical model. From Eq. (26) it is clear that the value of k where E maximizes corresponds to the observationally favored magnitude of k. Figure 3 depicts the variation of E with k for two different choices of r_{out}. From the figure we note that E maximizes when $k \simeq 0.15$ irrespective of the choice of r_{out} which is in agreement with our results obtained from χ^2 estimate.

- **Modified Nash–Sutcliffe Efficiency:** The presence of the squared term in the expression for Nash–Sutcliffe Efficiency makes it oversensitive to larger values of the luminosity. As a result, a modified version of the same (denoted by E_1) is put forward [112] which is given by,

$$E_1(k) = 1 - \frac{\sum_j \left|O_j - T_j\left(k, \{a_{min,j}, \cos i_{min,j}, \dot{M}_{min,j}\}\right)\right|}{\sum_j \left|O_j - O_{\rm av}\right|} \tag{27}$$

From Eq. (27) it is clear that the value of k where E_1 maximizes corresponds to the observationally favored magnitude of k. We note from Fig. 4 that $k \simeq 0.15$ maximizes E_1 which implies that the black holes in non-linear electrodynamics are more favored observationally compared to the Kerr scenario. This result holds good irrespective of the choice of r_{out} and is consistent with our previous findings.

- **Index of agreement and its modified form:** The Nash–Sutcliffe efficiency and its modified form is insensitive to the differences associated with the theoretical and the observed luminosities from the respective observed mean [112]. This inspires one to propose two more error estimators, namely the index of agreement and its modified form which takes care of this issue [113–115]. The index of agreement is given by

$$d(k) = 1 - \frac{\sum_j \left\{O_j - T_j\left(k, \{a_{min,j}, \cos i_{min,j}, \dot{M}_{min,j}\}\right)\right\}^2}{\sum_j \left\{\left|O_j - O_{\rm av}\right| + \left|T_j\left(k, \{a_{min,j}, \cos i_{min,j}, \dot{M}_{min,j}\}\right) - O_{\rm av}\right|\right\}^2} \tag{28}$$

In Eq. (28) the average value of the observed luminosities is given by $O_{\rm av}$. The denominator of Eq. (28) often referred to as the potential error is associated with the maximum departure of each pair of observed and theoretical luminosities from the observed mean $O_{\rm av}$. Once again, the presence of squared terms in the numerator makes the index of agreement oversensitive to higher values of optical luminosity. As a consequence, a modified version of the index of agreement is proposed which assumes the form,

$$d_1(k) = 1 - \frac{\sum_j \left|O_j - T_j\left(k, \{a_{min,j}, \cos i_{min,j}, \dot{M}_{min,j}\}\right)\right|}{\sum_j \left\{\left|O_j - O_{\rm av}\right| + \left|T_j\left(k, \{a_{min,j}, \cos i_{min,j}, \dot{M}_{min,j}\}\right) - O_{\rm av}\right|\right\}} \tag{29}$$

We note from Eq. (28) and Eq. (29) that the magnitude of k where the index of agreement and its modified form maximizes corresponds to the observationally favored value of k. Figures 5 and 6 respectively illustrate the variation of d and d_1 with respect to k for $r_{out} = 500r_g$ (left panel) and $r_{out} = 1000r_g$ (right panel). It is clear from the aforesaid figures that d and d_1 maximizes when $k \simeq 0.15$

regardless of the choice of r_{out}. This is in accordance with our earlier results which states that regular black holes with a Minkowski core are more favored compared to the Kerr black holes as far as optical observations of quasars are concerned. Thus, all the five error estimators indicate towards the same conclusion. It turns out that our results are in agreement with a previous study where we derived the magnitude of k from observations related to quasi-periodic oscillations (QPOs) in black holes [78]. It is interesting that two independent observations (BH continuum spectrum and QPOs) on completely different observational samples consistently favor similar magnitude of k. In an earlier work we studied the signatures of Bardeen black holes from the present quasar data. Bardeen black holes are examples of regular black holes with a de Sitter core arising in Einstein gravity coupled to non-linear electrodynamics. In that case error analysis showed that quasar optical data favors the Kerr scanario compared to black holes with a non-linear electrodynamics charge [77]. In the next section we report the spins of the quasars corresponding to the observationally favored magnitude of k (i.e. $k \simeq 0.15$).

4.2 Spins of the quasars

The present section gives an estimate of the spin of the quasars derived from their optical observations. We recall here that for a given k, every quasar has an observationally favored value of spin denoted by a_{min} discussed in Sect. 4. From the discussion in the last section we note that the χ^2 minimizes while the other errors maximize when $k \simeq 0.15$. We therefore report spins (a_{min}) corresponding to $k \simeq 0.15$ for the quasars in Table 1. For completeness we also report spins corresponding to $k = 0$ which in turn can be compared with previous observations.

It is important to note that the theoretical luminosity depends both on the inner disk radius (which in the present case is the marginally stable circular orbit r_{ms}) and the radius of the outer disk r_{out}. Since the flux emitted from the accretion disk peaks close to the r_{ms}, the luminosity is much more sensitive to the inner radius. Hence, the choice of r_{out} does not affect our observationally favored magnitude of k. However, for some quasars the choice of r_{out} does affect the value of a_{min} corresponding to $k = 0$ or $k \simeq 0.15$. We report spins of only those quasars in Table 1 whose a_{min} corresponding to $k = 0$ and $k \simeq 0.15$ remain invariant with r_{out}. The variation of a_{min} (for a given k) with r_{out} stems from the fact that we allowed the inclination angle and the accretion rate to vary while calculating the error estimators. Moreover, the theoretical luminosity is directly related to the temperature profile $T(r)$ which in turn depends on $\dot{M}/\mathcal{M}^2$. Hence the quasars for which this ratio is high, gets some contribution to the theoretical luminosity from the outer disk. This in turn alters the value of a_{min} for those quasars for a given k. In Table 1 we report the Kerr parameter of only those quasars whose spin remains unaltered with variation of r_{out}.

The spins of some of the quasars presented in Table 1 have been determined independently by other methods. We now compare our spin constraints with that of the previously estimated spins of the quasars. The spin of PG 0003+199 have been determined previously by several authors. For example, according to Keek et al. [116] the spin of PG 0003+199 turns out to be $a \sim 0.89 \pm 0.05$, while Walton et al. [117] reported the spin of PG 0003+199 to be $a \sim 0.83^{+0.09}_{-0.13}$. Based on the general relativistic disk reflection model [118,119]reported that the quasars PG 0003+199, PG 0050+124, PG 1244+026, PG 1404+226, PG 1440+356 are maximally spinning. These results are nearly consistent with our findings. Using polarimetric observations of AGNs [120] the spins of PG 0003+199, PG 0050+124, PG 0923+129, PG 2308+098, PG 1022+519, PG 1425+267, PG 1545+210, PG 1613+658 and PG 1704+608 have been determined. We note that our estimate of spin for the quasars PG 0003+199, PG 0050+124, PG 0923+129 and PG 2308+098 are in agreement with their results while our estimate of spin for PG 1022+519, PG 1425+267, PG 1545+210, PG 1613+658 and PG 1704+608 show some deviations. Bottacini et al. [121] reported that PG 1613+658 (Mrk 876) consists of a rotating black hole which is in accordance with our findings. According to [109] the spin of PG 1704+608 (3C 351) is $a < 0.998$ which is in agreement with our results.

5 Concluding remarks

The present paper investigates the nature of the continuum spectrum emitted by the accretion disk around regular black holes and aims to discern the viability of the regular black hole scenario compared to the Kerr scenario in GR. The regular black holes considered here are endowed with a Minkowski core and arises in Einstein gravity coupled to non-linear electrodynamics. Exploring the signatures of such black holes in astrophysical observations is interesting because they can potentially evade the $r = 0$ curvature singularity arising in GR. The regular black hole considered here has an exponential mass function and is characterized by the non-linear electrodynamics charge (magnetic monopole charge) parameter k and the spin parameter a. The continuum spectrum depends both on the metric parameters as well as the properties of the accretion flow. We work out the theoretical luminosity in such a background using the thin-disk approximation. This when compared with the optical observations of eighty Palomar Green quasars reveal that mildly charged regular black holes ($k \simeq 0.15$) with a Minkowski core are more favored compared to the Kerr scenario in GR. Our find-

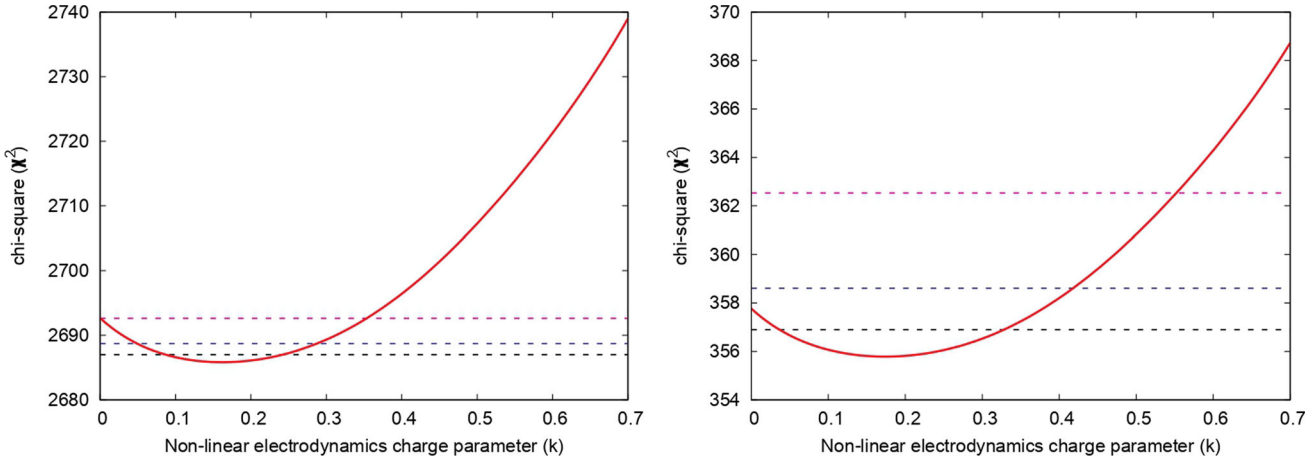

Fig. 2 The above figure illustrates the variation of χ^2 with the non-linear electrodynamics charge parameter k. This is shown for two choices of r_{out}, namely, $r_{out} = 500R_g$ (left panel) and $r_{out} = 1000R_g$ (right panel). The figure clearly shows that χ^2 minimizes for a small but non-trivial value of the magnetic monopole charge parameter $k \simeq 0.15$ irrespective of the choice of r_{out}. The 1-σ, 2-σ and 3-σ contours denoted by black, blue and magenta dashed lines respectively are plotted. The figure above indicates that large values of k are ruled out outside 99% confidence interval

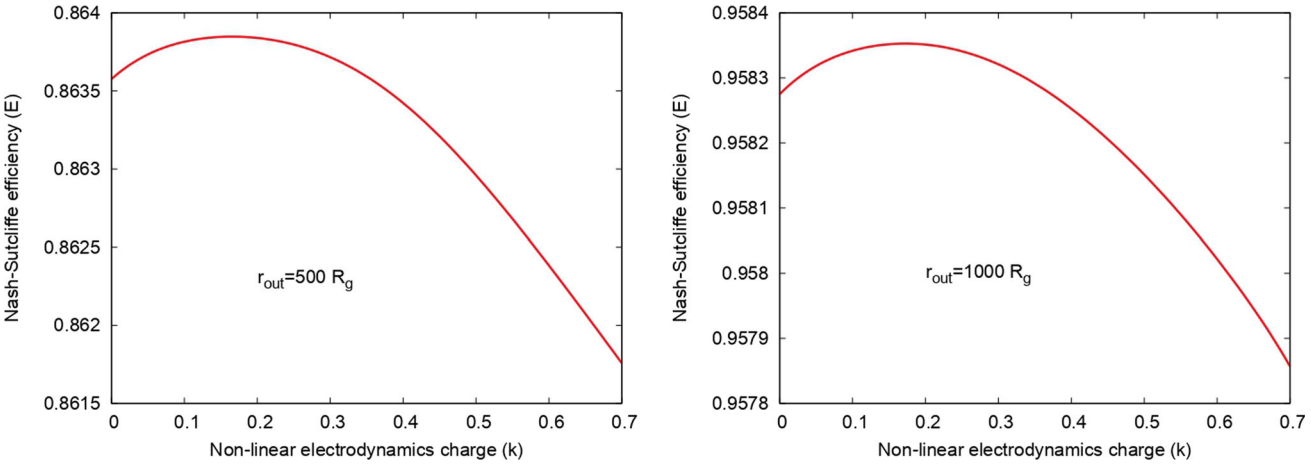

Fig. 3 The above figure illustrates the variation of the Nash–Sutcliffe Efficiency E with the non-linear electrodynamics charge parameter k. In the left panel the theoretical optical luminosity is computed with $r_{out} = 500r_g$ while the right panel corresponds to $r_{out} = 1000r_g$ for computing the theoretical optical luminosity. The figure shows that E maximizes for $k \simeq 0.15$ in agreement with our findings based on χ^2 analysis

ings are based on error estimators like χ^2, the Nash–Sutcliffe efficiency, the index of agreement and their modified forms. General relativity is however included within 3-σ and 2-σ confidence intervals depending on whether the outer radius is taken to be $r_{out} = 500r_g$ and $r_{out} = 1000r_g$ respectively.

Previously we studied the prospect of the present regular black hole scenario in explaining the observed quasi-periodic oscillations [78] and black hole shadow [122]. Our analysis indicates that most theoretical models proposed to explain the QPOs favor a small but non-trivial value of the magnetic monopole charge parameter k. Even the shadows of M87* and Sgr A* indicate towards a similar result. This is interesting since three independent observations with completely different observational samples consistently give rise to similar constraints on k. In particular, all the observations disfavor large values of k.

In an earlier work we performed the same analysis with Bardeen black holes (regular black holes with a de Sitter core arising in non-linear electrodynamics) [77] and noted that the Kerr scenario was more favored in that case. In this context it might be important to note that the Kerr solution arises in some alternative gravity models as well [123], and observational confirmation of the Kerr metric may not always indicate that GR is more favored. The present analysis also

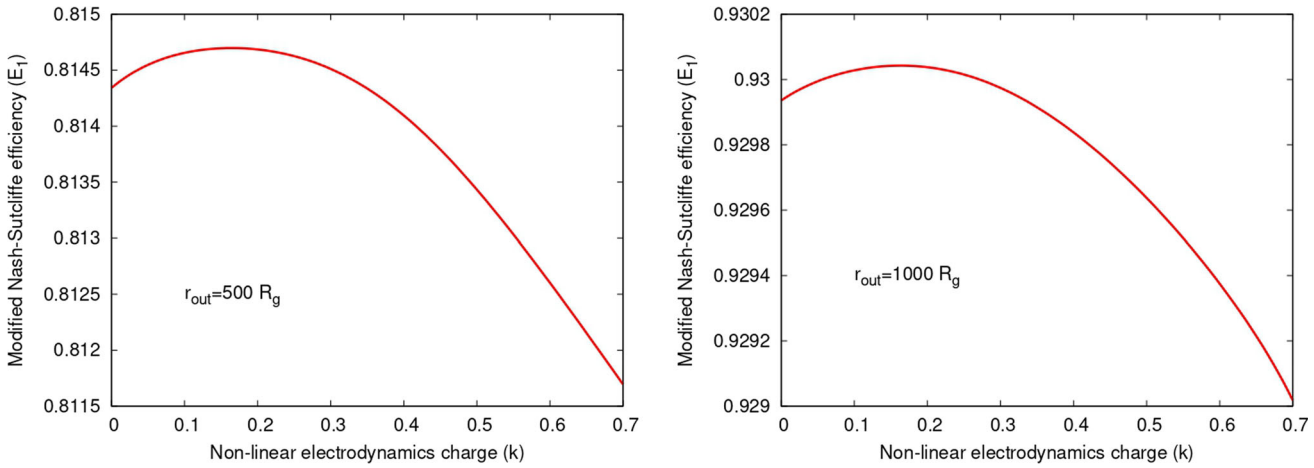

Fig. 4 In the figure the modified Nash–Sutcliffe Efficiency E_1 is plotted with the non-linear electrodynamics charge parameter k. In the left panel E_1 is plotted for $r_{out} = 500r_g$ while E_1 calculated with $r_{out} = 1000r_g$ is shown in the right panel. In both cases, E_1 maximizes for $k \simeq 0.15$ implying that regular black holes in non-linear electrodynamics are more favored compared to Kerr black holes in general relativity

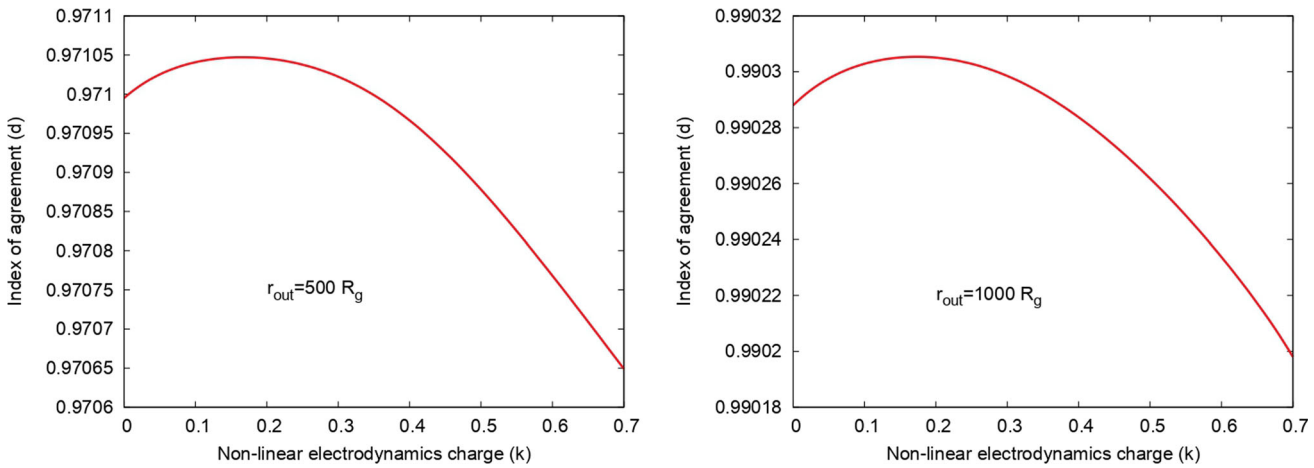

Fig. 5 The above figure plots the index agreement d with respect to the non-linear electrodynamics charge parameter k. The index of agreement computed with $r_{out} = 500r_g$ and $r_{out} = 1000r_g$ are shown in the left and the right panels respectively. Irrespective of the choice of r_{out}, d peaks at $k \simeq 0.15$ supporting the regular black hole case compared to the Kerr scenario in GR

allows us to establish constrains on the spins of some quasars which are more or less in agreement with previous estimates.

Before we conclude we would like to mention some of the shortcomings of the present analysis. First of all, the spectral energy distribution (SED) of quasars consists of contribution from the accretion disk, the corona, the jet and the dusty torus which are difficult to observe and model [106]. Deciphering the signatures of the various components from the SED is not easy which turns out to be a limitation in precise determination of the black hole parameters like mass, distance, spin or inclination. Second, the continuum spectrum depends not only on the background metric but also on the characteristics of the accretion flow. The thin-disk approximation assumes motion along the equatorial plane with negligible radial and vertical velocity. In order to model a realistic accretion flow these assumptions need to be relaxed. This requires a much more detailed modelling of the spectrum taking into account the dynamical evolution of the disk, the corona, the jet and the outflows. At present these issues are addressed by several phenomenological models which is beyond the scope of this work. Moreover, the present result is dependent on the observational sample. It is therefore instructive to carry out the present analysis with a different black hole sample. Apart from using a different black hole sample, it is worthwhile to investigate the viability of the regular black hole scenario with other astrophysical observations, namely, Fe-line method or gravitational waves. This in turn can establish independent constraints on the non-linear electrodynamics

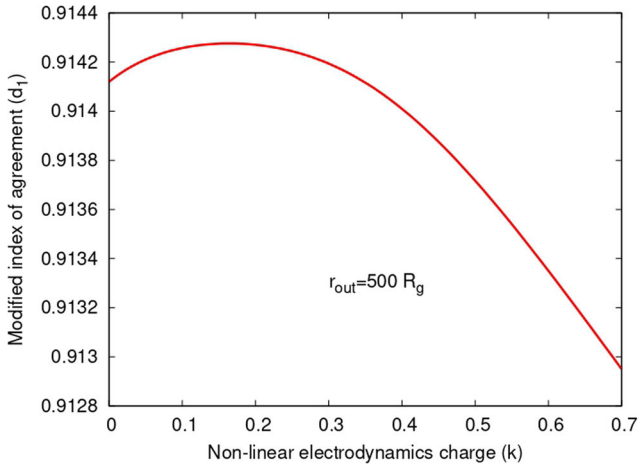

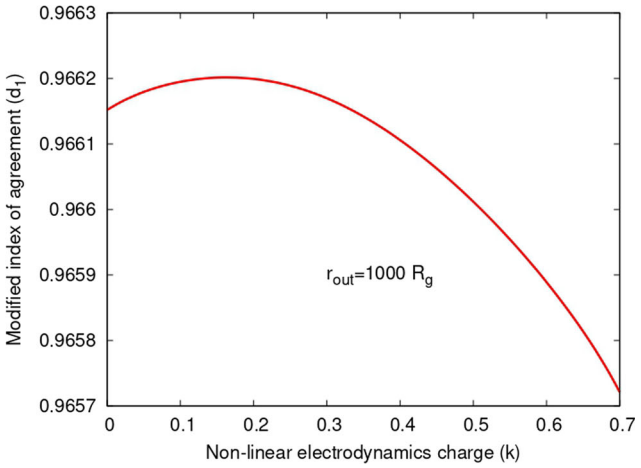

Fig. 6 The figure above depicts the variation of the modified index of agreement d_1 with the non-linear electrodynamics charge parameter k. In the left panel d_1 is computed with $r_{out} = 500r_g$ while in the right panel d_1 is evaluated with $r_{out} = 1000r_g$. In both cases d_1 maximizes for $k \simeq 0.15$ indicating that optical observations of quasars favor regular black holes in non-linear electrodynamics compared to the Kerr scenario in general relativity

Table 1 Estimates on spin parameters of the quasars corresponding to $k = 0$ and $k \simeq 0.15$

Object	log m	$a_{k=0}$	$a_{k=0.15}$
0003 + 199	6.88	0.99	0.95
0050 + 124	6.99	0.99	0.95
0923 + 129	6.82	0.99	0.95
0923 + 201	8.84	−0.4	0.3
1011 − 040	6.89	0.99	0.95
1022 + 519	6.63	0.99	0.95
1119 + 120	7.04	0.99	0.95
1244 + 026	6.15	0.99	0.95
1404 + 226	6.52	0.99	0.95
1425 + 267	9.53	0.7	0.5
1440 + 356	7.09	0.99	0.95
1535 + 547	6.78	0.99	0.95
1545 + 210	9.10	0.1	0.2
1552 + 085	7.17	0.99	0.95
1613 + 658	8.89	0.3	0.4
1704 + 608	9.29	−0.4	0.1
2130 + 099	7.49	0.99	0.95
2308 + 098	9.43	0.95	0.4

charge parameter, which can be compared with the present work. We leave this for a future work which will be reported elsewhere.

Acknowledgements Research of I.B. is funded by the Start-Up Research Grant from SERB, DST, Government of India (Reg. No. SRG/2021/000418).

Data availability The data underlying this article are taken from Davis and Laor (2011) [79] cited in the text.

Funded by SCOAP[3]. SCOAP[3] supports the goals of the International Year of Basic Sciences for Sustainable Development.

References

1. C.M. Will, Was Einstein right? Ann. Phys. **15**, 19–33 (2005). https://doi.org/10.1002/andp.200510170,10.1142/9789812700988_0008. arXiv:gr-qc/0504086 [gr-qc] [Annalen Phys. 518, 19 (2006)]
2. C.M. Will, Theory and experiment in gravitational physics (1993)
3. C.M. Will, The confrontation between general relativity and experiment. Living Rev. Relativ. **9**, 3 (2006). https://doi.org/10.12942/lrr-2006-3. arXiv:gr-qc/0510072 [gr-qc]
4. LIGO Scientific, VIRGO Collaboration, B.P. Abbott et al., GW170104: observation of a 50-solar-mass binary black hole coalescence at Redshift 0.2. Phys. Rev. Lett. **118**(22), 221101 (2017). https://doi.org/10.1103/PhysRevLett.118.221101, https://doi.org/10.1103/PhysRevLett.121.129901. arXiv:1706.01812 [gr-qc] [Erratum: Phys. Rev. Lett. 121(12), 129901 (2018)]
5. LIGO Scientific, Virgo Collaboration, B.P. Abbott et al., Binary black hole mergers in the first advanced LIGO observing

run. Phys. Rev. X **6**(4), 041015 (2016). https://doi.org/10.1103/PhysRevX.6.041015, https://doi.org/10.1103/PhysRevX.8.039903. arXiv:1606.04856 [gr-qc] [Erratum: Phys. Rev. X 8(3), 039903 (2018)]
6. LIGO Scientific, Virgo Collaboration, B.P. Abbott et al., GW151226: observation of gravitational waves from a 22-solar-mass binary black hole coalescence. Phys. Rev. Lett. **116**(24), 241103 (2016). https://doi.org/10.1103/PhysRevLett.116.241103. arXiv:1606.04855 [gr-qc]
7. LIGO Scientific, Virgo Collaboration, B.P. Abbott et al., Tests of general relativity with GW150914. Phys. Rev. Lett. **116**(22), 221101 (2016). https://doi.org/10.1103/PhysRevLett.116.221101, https://doi.org/10.1103/PhysRevLett.121.129902. arXiv:1602.03841 [gr-qc] [Erratum: Phys. Rev. Lett. 121(12), 129902 (2018)]
8. LIGO Scientific, Virgo Collaboration, B.P. Abbott et al., Observation of gravitational waves from a binary black hole merger. Phys. Rev. Lett. **116**(6), 061102 (2016). https://doi.org/10.1103/PhysRevLett.116.061102. arXiv:1602.03837 [gr-qc]
9. Event Horizon Telescope Collaboration, V.L. Fish, K. Akiyama, K.L. Bouman, A.A. Chael, M.D. Johnson, S.S. Doeleman, L. Blackburn, J.F.C. Wardle, W.T. Freeman, Observing- and imaging-active galactic nuclei with the event horizon telescope. Galaxies **4**(4), 54 (2016). https://doi.org/10.3390/galaxies4040054. arXiv:1607.03034 [astro-ph.IM]
10. Event Horizon Telescope Collaboration, K. Akiyama et al., First M87 event horizon telescope results. I. The shadow of the supermassive black hole. Astrophys. J. **875**(1), L1 (2019). https://doi.org/10.3847/2041-8213/ab0ec7
11. Event Horizon Telescope Collaboration, K. Akiyama et al., First M87 event horizon telescope results. II. Array and instrumentation. Astrophys. J. **875**(1), L2 (2019). https://doi.org/10.3847/2041-8213/ab0c96. arXiv:1906.11239 [astro-ph.IM]
12. Event Horizon Telescope Collaboration, K. Akiyama et al., First M87 event horizon telescope results. III. Data processing and calibration. Astrophys. J. **875**(1), L3 (2019). https://doi.org/10.3847/2041-8213/ab0c57. arXiv:1906.11240 [astro-ph.GA]
13. Event Horizon Telescope Collaboration, K. Akiyama et al., First M87 event horizon telescope results. IV. Imaging the central supermassive black hole. Astrophys. J. **875**(1), L4 (2019). https://doi.org/10.3847/2041-8213/ab0e85. arXiv:1906.11241 [astro-ph.GA]
14. Event Horizon Telescope Collaboration, K. Akiyama et al., First M87 event horizon telescope results. V. Physical origin of the asymmetric ring. Astrophys. J. **875** (1), L5 (2019). https://doi.org/10.3847/2041-8213/ab0f43. arXiv:1906.11242 [astro-ph.GA]
15. Event Horizon Telescope Collaboration, K. Akiyama et al., First M87 event horizon telescope results. VI. The shadow and mass of the central black hole. Astrophys. J. **875**(1), L6 (2019). https://doi.org/10.3847/2041-8213/ab1141
16. M. Milgrom, A modification of the Newtonian dynamics: implications for galaxies. Astrophys. J. **270**, 371–383 (1983). https://doi.org/10.1086/161131
17. M. Milgrom, R.H. Sanders, MOND and the Dearth of dark matter in ordinary elliptical galaxies. Astrophys. J. **599**, L25–L28 (2003). https://doi.org/10.1086/381138. arXiv:astro-ph/0309617 [astro-ph]
18. J. Bekenstein, M. Milgrom, Does the missing mass problem signal the breakdown of Newtonian gravity? Astrophys. J. **286**, 7–14 (1984). https://doi.org/10.1086/162570
19. Supernova Cosmology Project Collaboration, S. Perlmutter et al., Measurements of Omega and Lambda from 42 high redshift supernovae. Astrophys. J. **517**, 565–586 (1999). https://doi.org/10.1086/307221. arXiv:astro-ph/9812133 [astro-ph]
20. Supernova Search Team Collaboration, A.G. Riess et al., Observational evidence from supernovae for an accelerating universe and a cosmological constant. Astron. J. **116**, 1009–1038 (1998). https://doi.org/10.1086/300499. arXiv:astro-ph/9805201
21. S.W. Hawking, G.F.R. Ellis, *The Large Scale Structure of Space-Time. Cambridge Monographs on Mathematical Physics* (Cambridge University Press, Cambridge, 2011)
22. S. Nojiri, S.D. Odintsov, Modified gravity with negative and positive powers of the curvature: unification of the inflation and of the cosmic acceleration. Phys. Rev. D **68**, 123512 (2003). https://doi.org/10.1103/PhysRevD.68.123512. arXiv:hep-th/0307288 [hep-th]
23. S. Nojiri, S.D. Odintsov, Modified f(R) gravity consistent with realistic cosmology: From matter dominated epoch to dark energy universe. Phys. Rev. D **74**, 086005 (2006). https://doi.org/10.1103/PhysRevD.74.086005. arXiv:hep-th/0608008 [hep-th]
24. S. Capozziello, S. Nojiri, S.D. Odintsov, A. Troisi, Cosmological viability of f(R)-gravity as an ideal fluid and its compatibility with a matter dominated phase. Phys. Lett. B **639**, 135–143 (2006). https://doi.org/10.1016/j.physletb.2006.06.034. arXiv:astro-ph/0604431 [astro-ph]
25. C. Lanczos, Electricity as a natural property of Riemannian geometry. Rev. Mod. Phys. **39**, 716–736 (1932). https://doi.org/10.1103/RevModPhys.39.716
26. C. Lanczos, A remarkable property of the Riemann–Christoffel tensor in four dimensions. Ann. Math. **39**, 842–850 (1938). https://doi.org/10.2307/1968467
27. D. Lovelock, The Einstein tensor and its generalizations. J. Math. Phys. **12**, 498–501 (1971). https://doi.org/10.1063/1.1665613
28. T. Padmanabhan, D. Kothawala, Lanczos–Lovelock models of gravity. Phys. Rep. **531**, 115–171 (2013). https://doi.org/10.1016/j.physrep.2013.05.007. arXiv:1302.2151 [gr-qc]
29. T. Shiromizu, K.-I. Maeda, M. Sasaki, The Einstein equation on the 3-brane world. Phys. Rev. D **62**, 024012 (2000). https://doi.org/10.1103/PhysRevD.62.024012. arXiv:gr-qc/9910076 [gr-qc]
30. N. Dadhich, R. Maartens, P. Papadopoulos, V. Rezania, Black holes on the brane. Phys. Lett. B **487**, 1–6 (2000). https://doi.org/10.1016/S0370-2693(00)00798-X. arXiv:hep-th/0003061
31. T. Harko, M.K. Mak, Vacuum solutions of the gravitational field equations in the brane world model. Phys. Rev. D **69**, 064020 (2004). https://doi.org/10.1103/PhysRevD.69.064020. arXiv:gr-qc/0401049 [gr-qc]
32. T.R.P. Carames, M.E.X. Guimaraes, J.M. Hoff da Silva, Effective gravitational equations for $f(R)$ braneworld models. Phys. Rev. D **87**(10), 106011 (2013). https://doi.org/10.1103/PhysRevD.87.106011. arXiv:1205.4980 [gr-qc]
33. G.W. Horndeski, Second-order scalar-tensor field equations in a four-dimensional space. Int. J. Theor. Phys. **10**, 363–384 (1974). https://doi.org/10.1007/BF01807638
34. T.P. Sotiriou, S.-Y. Zhou, Black hole hair in generalized scalar-tensor gravity. Phys. Rev. Lett. **112**, 251102 (2014). https://doi.org/10.1103/PhysRevLett.112.251102. arXiv:1312.3622 [gr-qc]
35. E. Babichev, C. Charmousis, A. Lehébel, Black holes and stars in Horndeski theory. Class. Quanum Gravity **33**(15), 154002 (2016). https://doi.org/10.1088/0264-9381/33/15/154002. arXiv:1604.06402 [gr-qc]
36. C. Charmousis, M. Tsoukalas, Lovelock Galileons and black holes. Phys. Rev. D **92**(10), 104050 (2015). https://doi.org/10.1103/PhysRevD.92.104050. arXiv:1506.05014 [gr-qc]
37. P. Horava, E. Witten, Heterotic and type I string dynamics from eleven-dimensions. Nucl. Phys. B **460**, 506–524 (1996). https://doi.org/10.1016/0550-3213(95)00621-4. arXiv:hep-th/9510209 [hep-th]
38. P. Horava, E. Witten, Eleven-dimensional supergravity on a manifold with boundary. Nucl. Phys. B **475**, 94–114 (1996). https://doi.org/10.1016/0550-3213(96)00308-2. arXiv:hep-th/9603142 [hep-th]

39. J. Polchinski, *String Theory. Vol. 1: An Introduction to the Bosonic String. Cambridge Monographs on Mathematical Physics* (Cambridge University Press, Cambridge, 2007). https://doi.org/10.1017/CBO9780511816079
40. J. Polchinski, *String Theory. Vol. 2: Superstring Theory and Beyond. Cambridge Monographs on Mathematical Physics* (Cambridge University Press, Cambridge, 2007). https://doi.org/10.1017/CBO9780511618123
41. A. Ashtekar, T. Pawlowski, P. Singh, Quantum nature of the big bang. Phys. Rev. Lett. **96**, 141301 (2006). https://doi.org/10.1103/PhysRevLett.96.141301. arXiv:gr-qc/0602086 [gr-qc]
42. A. Ashtekar, T. Pawlowski, P. Singh, Quantum nature of the big bang: an analytical and numerical investigation. I. Phys. Rev. D **73**, 124038 (2006). https://doi.org/10.1103/PhysRevD.73.124038. arXiv:gr-qc/0604013
43. A. Ashtekar, T. Pawlowski, P. Singh, Quantum nature of the big bang: improved dynamics. Phys. Rev. D **74**, 084003 (2006). https://doi.org/10.1103/PhysRevD.74.084003. arXiv:gr-qc/0607039
44. D. Kothawala, Minimal length and small scale structure of spacetime. Phys. Rev. D **88**(10), 104029 (2013). https://doi.org/10.1103/PhysRevD.88.104029. arXiv:1307.5618 [gr-qc]
45. D. Kothawala, Small scale structure of spacetime in presence of a minimal length. J. Phys. Conf. Ser. **600**(1), 012069 (2015). https://doi.org/10.1088/1742-6596/600/1/012069
46. S. Ansoldi, Spherical black holes with regular center: a review of existing models including a recent realization with Gaussian sources. in *Conference on Black Holes and Naked Singularities*, Vol. 2 (2008). arXiv:0802.0330 [gr-qc]
47. E.B. Gliner, Algebraic properties of the energy-momentum tensor and vacuum-like states o^+ matter. Sov. J. Exp. Theor. Phys. **22**, 378 (1966)
48. Z.-Y. Fan, X. Wang, Construction of regular black holes in general relativity. Phys. Rev. D **94**(12), 124027 (2016). https://doi.org/10.1103/PhysRevD.94.124027. arXiv:1610.02636 [gr-qc]
49. K.A. Bronnikov, Regular magnetic black holes and monopoles from nonlinear electrodynamics. Phys. Rev. D **63**, 044005 (2001). https://doi.org/10.1103/PhysRevD.63.044005. arXiv:gr-qc/0006014
50. A. Borde, Regular black holes and topology change. Phys. Rev. D **55**, 7615–7617 (1997). https://doi.org/10.1103/PhysRevD.55.7615. arXiv:gr-qc/9612057
51. C. Barrabes, V.P. Frolov, How many new worlds are inside a black hole? Phys. Rev. D **53**, 3215–3223 (1996). https://doi.org/10.1103/PhysRevD.53.3215. arXiv:hep-th/9511136
52. E. Ayon-Beato, A. Garcia, Nonsingular charged black hole solution for nonlinear source. Gen. Relativ. Gravit. **31**, 629–633 (1999). https://doi.org/10.1023/A:1026640911319. arXiv:gr-qc/9911084
53. A. Bonanno, M. Reuter, Renormalization group improved black hole space-times. Phys. Rev. D **62**, 043008 (2000). https://doi.org/10.1103/PhysRevD.62.043008. arXiv:hep-th/0002196
54. P. Nicolini, A. Smailagic, E. Spallucci, Noncommutative geometry inspired Schwarzschild black hole. Phys. Lett. B **632**, 547–551 (2006). https://doi.org/10.1016/j.physletb.2005.11.004. arXiv:gr-qc/0510112
55. Y.S. Myung, Y.-W. Kim, Y.-J. Park, Quantum cooling evaporation process in regular black holes. Phys. Lett. B **656**, 221–225 (2007). https://doi.org/10.1016/j.physletb.2007.09.056. arXiv:gr-qc/0702145
56. S.A. Hayward, Formation and evaporation of nonsingular black holes. Phys. Rev. Lett. **96**, 031103 (2006). https://doi.org/10.1103/PhysRevLett.96.031103
57. V.P. Frolov, M.A. Markov, V.F. Mukhanov, Black holes as possible sources of closed and semiclosed worlds. Phys. Rev. D **41**, 383 (1990). https://doi.org/10.1103/PhysRevD.41.383
58. V.F. Mukhanov, R.H. Brandenberger, A nonsingular universe. Phys. Rev. Lett. **68**, 1969–1972 (1992). https://doi.org/10.1103/PhysRevLett.68.1969
59. R.H. Brandenberger, V.F. Mukhanov, A. Sornborger, A cosmological theory without singularities. Phys. Rev. D **48**, 1629–1642 (1993). https://doi.org/10.1103/PhysRevD.48.1629. arXiv:gr-qc/9303001
60. H. Culetu, On a regular charged black hole with a nonlinear electric source. Int. J. Theor. Phys. **54**(8), 2855–2863 (2015). https://doi.org/10.1007/s10773-015-2521-6. arXiv:1408.3334 [gr-qc]
61. M.R. Brown, Is quantum gravity finite?, in *Oxford Conference on Quantum Gravity* (1980)
62. J.W. Moffat, Quantum gravity resolution to the cosmological constant problem. arXiv:hep-ph/0102088
63. E. Newman, A. Janis, Note on the Kerr spinning particle metric. J. Math. Phys. **6**, 915–917 (1965). https://doi.org/10.1063/1.1704350
64. M. Azreg-Aïnou, Generating rotating regular black hole solutions without complexification. Phys. Rev. D **90**(6), 064041 (2014). https://doi.org/10.1103/PhysRevD.90.064041. arXiv:1405.2569 [gr-qc]
65. M. Azreg-Aïnou, From static to rotating to conformal static solutions: Rotating imperfect fluid wormholes with(out) electric or magnetic field. Eur. Phys. J. C **74**(5), 2865 (2014). https://doi.org/10.1140/epjc/s10052-014-2865-8. arXiv:1401.4292 [gr-qc]
66. M. Azreg-Ainou, Regular and conformal regular cores for static and rotating solutions. Phys. Lett. B **730**, 95–98 (2014). https://doi.org/10.1016/j.physletb.2014.01.041. arXiv:1401.0787 [gr-qc]
67. S.G. Ghosh, A nonsingular rotating black hole. Eur. Phys. J. C **75**(11), 532 (2015). https://doi.org/10.1140/epjc/s10052-015-3740-y. arXiv:1408.5668 [gr-qc]
68. R. Kumar, S.G. Ghosh, Photon ring structure of rotating regular black holes and no-horizon spacetimes. Class. Quantum Gravity **38**(8), 8 (2021). https://doi.org/10.1088/1361-6382/abdd48. arXiv:2004.07501 [gr-qc]
69. R. Kumar, A. Kumar, S.G. Ghosh, Testing rotating regular metrics as candidates for astrophysical black holes. Astrophys. J. **896**(1), 89 (2020). https://doi.org/10.3847/1538-4357/ab8c4a. arXiv:2006.09869 [gr-qc]
70. A. Allahyari, M. Khodadi, S. Vagnozzi, D.F. Mota, Magnetically charged black holes from non-linear electrodynamics and the Event Horizon Telescope. JCAP **02**, 003 (2020). https://doi.org/10.1088/1475-7516/2020/02/003. arXiv:1912.08231 [gr-qc]
71. Z. Stuchlík, J. Schee, Circular geodesic of Bardeen and Ayon–Beato–Garcia regular black-hole and no-horizon spacetimes. Int. J. Mod. Phys. D **24**(02), 1550020 (2014). https://doi.org/10.1142/S0218271815500200. arXiv:1501.00015 [astro-ph.HE]
72. J. Schee, Z. Stuchlik, Gravitational lensing and ghost images in the regular Bardeen no-horizon spacetimes. JCAP **06**, 048 (2015). https://doi.org/10.1088/1475-7516/2015/06/048. arXiv:1501.00835 [astro-ph.HE]
73. J. Schee, Z. Stuchlík, Profiled spectral lines generated by Keplerian discs orbiting in the Bardeen and Ayòn–Beato–Garcìa spacetimes. Class. Quantum Gravity **33**(8), 085004 (2016). https://doi.org/10.1088/0264-9381/33/8/085004. arXiv:1604.00632 [gr-qc]
74. Z. Stuchlík, J. Schee, Shadow of the regular Bardeen black holes and comparison of the motion of photons and neutrinos. Eur. Phys. J. C **79**(1), 44 (2019). https://doi.org/10.1140/epjc/s10052-019-6543-8
75. J. Schee, Z. Stuchlik, Profiled spectral lines of Keplerian rings orbiting in the regular Bardeen black hole spacetimes. Eur. Phys. J. C **79**(12), 988 (2019). https://doi.org/10.1140/epjc/s10052-019-7420-1. arXiv:1908.07197 [gr-qc]
76. I. Banerjee, Deciphering signatures of Bardeen black holes from the observed quasi-periodic oscillations. JCAP **05**(05),

020 (2022). https://doi.org/10.1088/1475-7516/2022/05/020. arXiv:2201.00679 [gr-qc]
77. I. Banerjee, V.S. Chawan, B. Mandal, S.K. Sahoo, S. SenGupta, Quasar continuum spectrum disfavors black holes with a magnetic monopole charge. Phys. Rev. D **105**(6), 064073 (2022). https://doi.org/10.1103/PhysRevD.105.064073. arXiv:2112.05385 [gr-qc]
78. I. Banerjee, Testing black holes in non-linear electrodynamics from the observed quasi-periodic oscillations. JCAP **08**(08), 034 (2022). https://doi.org/10.1088/1475-7516/2022/08/034. arXiv:2203.10890 [gr-qc]
79. S.W. Davis, A. Laor, The radiative efficiency of accretion flows in individual AGN. Astrophys. J. **728**, 98 (2011). https://doi.org/10.1088/0004-637X/728/2/98. arXiv:1012.3213 [astro-ph.CO]
80. I.D. Novikov, K.S. Thorne, Astrophysics of black holes, in *Black Holes (Les Astres Occlus)*. ed. by C. Dewitt, B.S. Dewitt (Gordon and Breach, Paris, 1973), pp.343–450
81. D.N. Page, K.S. Thorne, Disk-accretion onto a black hole. time-averaged structure of accretion disk. Astrophys. J. **191**, 499–506 (1974). https://doi.org/10.1086/152990
82. E. Ayon-Beato, A. Garcia, The Bardeen model as a nonlinear magnetic monopole. Phys. Lett. B **493**, 149–152 (2000). https://doi.org/10.1016/S0370-2693(00)01125-4. arXiv:gr-qc/0009077
83. I.H. Salazar, A. Garcia, J. Plebanski, Duality rotations and type *D* solutions to Einstein equations with nonlinear electromagnetic sources. J. Math. Phys. **28**, 2171–2181 (1987). https://doi.org/10.1063/1.527430
84. K.A. Bronnikov, Comment on "Construction of regular black holes in general relativity". Phys. Rev. D **96**(12), 128501 (2017). https://doi.org/10.1103/PhysRevD.96.128501. arXiv:1712.04342 [gr-qc]
85. B. Toshmatov, Z. Stuchlík, B. Ahmedov, Comment on "Construction of regular black holes in general relativity". Phys. Rev. D **98**(2), 028501 (2018). https://doi.org/10.1103/PhysRevD.98.028501. arXiv:1807.09502 [gr-qc]
86. H. Culetu, On a regular modified Schwarzschild spacetime. arXiv:1305.5964 [gr-qc]
87. C. Ganguly, S. SenGupta, Penrose process in a charged axion-dilaton coupled black hole. Eur. Phys. J. C **76**(4), 213 (2016). https://doi.org/10.1140/epjc/s10052-016-4058-0. arXiv:1401.6826 [hep-th]
88. G.W. Gibbons, D.A. Rasheed, Sl(2, R) invariance of non-linear electrodynamics coupled to an axion and a dilaton. Phys. Lett. B **365**, 46–50 (1996). https://doi.org/10.1016/0370-2693(95)01272-9. arXiv:hep-th/9509141
89. S.R. Valluri, D.J. Jeffrey, R.M. Corless, Some applications of the Lambert W function to physics. Can. J. Phys. **78**, 823–831 (2000). https://doi.org/10.1139/p00-065
90. P. Boonserm, M. Visser, Bounding the greybody factors for Schwarzschild black holes. Phys. Rev. D **78**, 101502 (2008). https://doi.org/10.1103/PhysRevD.78.101502. arXiv:0806.2209 [gr-qc]
91. P. Boonserm, M. Visser, Quasi-normal frequencies: key analytic results. JHEP **03**, 073 (2011). https://doi.org/10.1007/JHEP03(2011)073. arXiv:1005.4483 [math-ph]
92. P. Boonserm, T. Ngampitipan, M. Visser, Regge–Wheeler equation, linear stability, and greybody factors for dirty black holes. Phys. Rev. D **88**, 041502 (2013). https://doi.org/10.1103/PhysRevD.88.041502. arXiv:1305.1416 [gr-qc]
93. P. Boonserm, T. Ngampitipan, A. Simpson, M. Visser, Exponential metric represents a traversable wormhole. Phys. Rev. D **98**(8), 084048 (2018). https://doi.org/10.1103/PhysRevD.98.084048. arXiv:1805.03781 [gr-qc]
94. H. Sonoda, Solving renormalization group equations with the Lambert *W* function. Phys. Rev. D **87**(8), 085023 (2013). https://doi.org/10.1103/PhysRevD.87.085023. arXiv:1302.6069 [hep-th]
95. H. Sonoda, Analytic form of the effective potential in the large *N* limit of a real scalar theory in four dimensions. arXiv:1302.6059 [hep-th]
96. R. Kumar, S.G. Ghosh, Black hole parameters estimation from its shadow. arXiv:1811.01260 [gr-qc]
97. D. Ayzenberg, N. Yunes, Black hole continuum spectra as a test of general relativity: quadratic gravity. Class. Quantum Gravity **34**(11), 115003 (2017). https://doi.org/10.1088/1361-6382/aa6dbc. arXiv:1701.07003 [gr-qc]
98. S. Kaspi, P.S. Smith, H. Netzer, D. Maoz, B.T. Jannuzi, U. Giveon, Reverberation measurements for 17 quasars and the size mass luminosity relations in active galactic nuclei. Astrophys. J. **533**, 631 (2000). https://doi.org/10.1086/308704. arXiv:astro-ph/9911476 [astro-ph]
99. S. Kaspi, D. Maoz, H. Netzer, B.M. Peterson, M. Vestergaard, B.T. Jannuzi, The Relationship between luminosity and broad-line region size in active galactic nuclei. Astrophys. J. **629**, 61–71 (2005). https://doi.org/10.1086/431275. arXiv:astro-ph/0504484
100. T.A. Boroson, R.F. Green, The emission-line properties of low-redshift quasi-stellar objects. Astrophys. J. Suppl. **80**, 109 (1992). https://doi.org/10.1086/191661
101. B.M. Peterson et al., Central masses and broad-line region sizes of active galactic nuclei. II. A Homogeneous analysis of a large reverberation-mapping database. Astrophys. J. **613**, 682–699 (2004). https://doi.org/10.1086/423269. arXiv:astro-ph/0407299
102. G. Neugebauer, R.F. Green, K. Matthews, M. Schmidt, B.T. Soifer, J. Bennett, Continuum energy distributions of quasars in the Palomar–Green Survey. Astrophys. J. **63**
103. A. Baskin, A. Laor, What controls the C IV line profile in active galactic nuclei?. Mon. Not. Roy. Astron. Soc. **356**, 1029–1044 (2005). https://doi.org/10.1111/j.1365-2966.2004.08525.x. arXiv:astro-ph/0409196
104. J.E. Scott, G.A. Kriss, M. Brotherton, R.F. Green, J. Hutchings, J.M. Shull, W. Zheng, A composite extreme ultraviolet QSO spectrum from FUSE. Astrophys. J. **615**, 135–149 (2004). https://doi.org/10.1086/422336. arXiv:astro-ph/0407203 [astro-ph]
105. W.N. Brandt, A. Laor, B.J. Wills, On the nature of soft X-ray weak quasistellar objects. Astrophys. J. **528**, 637–649 (2000). https://doi.org/10.1086/308207. arXiv:astro-ph/9908016
106. L. Brenneman, Measuring supermassive black hole spins in active galactic nuclei. arXiv:1309.6334 [astro-ph.HE]
107. R. Antonucci, Unified models for active galactic nuclei and quasars. Annu. Rev. Astron. Astrophys. **31**, 473–521 (1993). https://doi.org/10.1146/annurev.aa.31.090193.002353
108. S. Wu, Y. Lu, F. Zhang, Y. Lu, Radiative efficiency of disk accretion in individual SDSS QSOs. Mon. Not. R. Astron. Soc. **436**, 3271 (2013). https://doi.org/10.1093/mnras/stt1811. arXiv:1310.0560 [astro-ph.CO]
109. M.Y. Piotrovich, Y.N. Gnedin, T.M. Natsvlishvili, S.D. Buliga, Constraints on spin of a supermassive black hole in quasars with big blue bump. ApSS **362**, 231 (2017). https://doi.org/10.1007/s10509-017-3216-7. arXiv:1711.07272
110. Y. Avni, Energy spectra of X-ray clusters of galaxies. ApJ **210**, 642–646 (1976). https://doi.org/10.1086/154870
111. J. Nash, J. Sutcliffe, River flow forecasting through conceptual models part I—a discussion of principles. J. Hydrol. **10**(3), 282–290 (1970). http://www.sciencedirect.com/science/article/pii/0022169470902556
112. D.R. Legates, G.J. McCabe, Evaluating the use of "goodness-of-fit" measures in hydrologic and hydroclimatic model validation. Water Resour. Res. **35**(1), 233–241 (1999). https://doi.org/10.1029/1998WR900018

113. P. Krause, D.P. Boyle, F. Bäse, Comparison of different efficiency criteria for hydrological model assessment. Adv. Geosci. **5**, 89–97 (2005)
114. C.J. Willmott, On the evaluation of model performance in physical geography, in *Spatial Statistics and Models*, pp. 443–460 (Springer, 1984)
115. C.J. Willmott, On the validation of models. Phys. Geogr. **2**(2), 184–194 (1981). https://doi.org/10.1080/02723646.1981.10642213
116. L. Keek, D.R. Ballantyne, Revealing the accretion disc corona in Mrk 335 with multi-epoch X-ray spectroscopy. Mon. Not. R. Astron. Soc. **456**(3), 2722–2734 (2016). https://doi.org/10.1093/mnras/stv2882. arXiv:1508.06994 [astro-ph.HE]
117. D.J. Walton, E. Nardini, A.C. Fabian, L.C. Gallo, R.C. Reis, Suzaku observations of 'bare' active galactic nuclei. Mon. Not. R. Astron. Soc. **428**, 2901 (2013). https://doi.org/10.1093/mnras/sts227. arXiv:1210.4593 [astro-ph.HE]
118. R.R. Ross, A.C. Fabian, A comprehensive range of X-ray ionized reflection models. Mon. Not. R. Astron. Soc. **358**, 211–216 (2005). https://doi.org/10.1111/j.1365-2966.2005.08797.x. arXiv:astro-ph/0501116
119. J. Crummy, A.C. Fabian, L. Gallo, R. Ross, An explanation for the soft X-ray excess in agn. Mon. Not. R. Astron. Soc. **365** , 1067–1081 (2006). https://doi.org/10.1111/j.1365-2966.2005.09844.x. arXiv:astro-ph/0511457 [astro-ph]
120. V.L. Afanasiev, Yu.N. Gnedin, MYu. Piotrovich, S.D. Buliga, T.M. Natsvlishvili, Determination of supermassive black hole spins based on the standard Shakura–Sunyaev accretion disk model and polarimetric observations. Astron. Lett. **44**(6), 362–369 (2018). https://doi.org/10.1134/S1063773718060014
121. E. Bottacini, E. Orlando, J. Greiner, M. Ajello, I. Moskalenko, M. Persic, An extreme gravitationally redshifted iron line at 4.8 keV in Mrk 876. Astrophys. J. **798**, L14 (2015). https://doi.org/10.1088/2041-8205/798/1/L14. arXiv:1412.3112 [astro-ph.HE]
122. I. Banerjee, S. Sau, S. SenGupta, Signatures of regular black holes from the shadow of Sgr A* and M87*. arXiv:2206.12125 [gr-qc]
123. D. Psaltis, D. Perrodin, K.R. Dienes, I. Mocioiu, Kerr black holes are not unique to general relativity. Phys. Rev. Lett. **100**, 091101 (2008). https://doi.org/10.1103/PhysRevLett.100.091101. arXiv:0710.4564 [astro-ph]